

Efficient adaptation of complex-valued noiselet sensing matrices for compressed single-pixel imaging

Anna Pastuszczak^{1,*}, Bartłomiej Szczygieł², Michał Mikołajczyk¹, and Rafał Kotyński¹

¹University of Warsaw, Faculty of Physics, Pasteura 7, 02-093, Warsaw, Poland

²University of Warsaw, College of Inter-Faculty Individual Studies in Mathematics and Natural Sciences, Żwirki i Wigury 93, 02-089 Warsaw, Poland

*Corresponding author: apastuszczak@igf.fuw.edu.pl

Minimal mutual coherence of discrete noiselets and Haar wavelets makes this pair of bases an essential choice for the measurement and compression matrices in compressed-sensing-based single-pixel detectors. In this paper we propose an efficient way of using complex-valued and non-binary noiselet functions for object sampling in single-pixel cameras with binary spatial light modulators and incoherent illumination. The proposed method allows to determine m complex noiselet coefficients from $m + 1$ binary sampling measurements. Further, we introduce a modification to the complex fast noiselet transform, which enables computationally-efficient real-time generation of the binary noiselet-based patterns using efficient integer calculations on bundled patterns. The proposed method is verified experimentally with a single-pixel camera system using a binary spatial light modulator.

1 Introduction

Compressed sensing (CS) [1, 2] is a technique of recovering a signal from an incomplete measurement based on an assumption that the signal has a sparse representation in a certain domain, for instance in some wavelet basis. In optics, CS has been initially applied for computational ghost imaging [3–5] giving rise to a novel image acquisition technique often referred to as single-pixel camera (SPC) [6], which allows for capturing images with a sole bucket detector rather than with a high-resolution array of detectors. This architecture opens the way for economic electro-optical imaging systems for infrared wavelengths [7], as well as for imaging in more exotic ranges of electromagnetic radiation, such as terahertz [8, 9] or millimeter waves [10]. Full color imaging [11], spectral imaging [12], Stokes polarimetric imaging [13], and imaging of three-dimensional objects [14–17] have been also demonstrated. The range of research directions related to the use of CS expands rapidly, including lidar imaging [18], compressive holography [19, 20], sparse sub-wavelength imaging [21, 22], compressive pattern recognition [23], rapid MRI diagnostics [24, 25] and imaging through scattering media such as a biological tissue [26]. Recently, a continuous real-time video recording at 10 Hz with SPC has been also reported [27].

The common element of CS-based imaging techniques is the use of spatially modulated illumination or aperture. This modulation is frequently achieved with binary spatial light modulators (SLM), for instance with micromirror devices (DMD). The choice of the sampling functions displayed by the SLM depends on the basis, in which the sampled image has a sparse representation. Indeed, the minimal number of measurements necessary to recover the image is a function of the second power of the coherence between these two bases.

As most of the real-world images are compressible in the wavelet domains, the application of sensing matrices incoherent with wavelets into CS-based imaging systems is essential. Presently, the sensing matrices are usually either based on Hadamard matrices or generated randomly. The Hadamard matrices are both easy to calculate and to display on a binary SLM, however their coherence with commonly used families of wavelets is rather high. The randomly generated patterns are acceptably incoherent with most of the image compression bases, however the necessity of storing the huge sensing matrix in the computer memory during the reconstruction of the image sets considerable limits on the resolution of the imaging system.

These problems are both overcome by sampling the images with noiselet functions [28]. Discrete noiselets take values from four-element complex sets, and importantly for CS with real-world images, are perfectly incoherent with Haar wavelet basis. A unitary noiselet matrix is fast to calculate. A way to calculate the fast noiselet transform (FNT) stems directly from the matrix definition. These properties, which we will overview in more depth in Section 3, decide upon the interest in the use of noiselets for SPC and are our motivation for the present work.

In this paper we focus on the efficient application of noiselet functions for SPC architectures. In a SPC set-up with incoherent illumination, light carries a nonnegative real intensity signal. Together with a binary spatial modulation which is respectively represented with real binary functions, the use of more general complex CS measurement matrices is not straightforward. We propose an efficient method which allows to determine m complex noiselet coefficients from $m + 1$ measurements with non-negative binary sampling patterns.

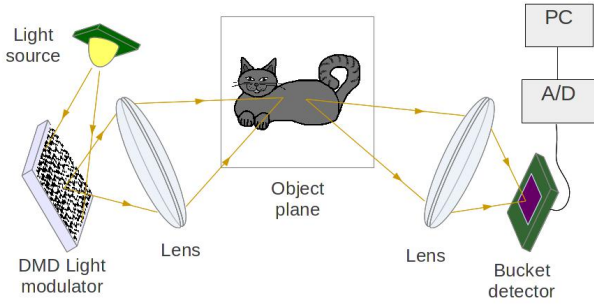


Figure 1: Schematic view of a single-pixel camera.

2 Compressed imaging

A schematic view of a typical single-pixel sparse imaging set-up with incoherent illumination is illustrated in Fig. 1. The system consists of a light source, a SLM, imaging lenses, and a bucket detector. The SLM is used for illuminating the object plane with structured light consisting of a series of binary patterns. Simultaneously, the combined images of the patterns and the object are projected onto a single-pixel detector, which measures their total intensities. Following, the results are digitised, stored and further processed using a PC.

Let Y be a vector of length m containing all the measurements captured by the bucket detector. Then, every measurement y_j ($1 \leq j \leq m$) within Y is a dot product of a vector ϕ_j representing the brightness of the consecutive pixels of the j -th pattern displayed by the SLM and of a vector X representing the reflectance (or transmittance) of the corresponding pixels of the image placed in the object plane:

$$y_j = \langle \phi_j, X \rangle. \quad (1)$$

A $m \times n$ matrix Φ , whose rows consist of all the patterns ϕ_j , is called a measurement or a sensing matrix.

In order to reconstruct the original image X from the set of measurements Y , one needs to solve a system of linear equations:

$$Y = \Phi \cdot X. \quad (2)$$

In the case of under-sampled image sensing, i.e. when $m < n$, Eq. (2) has an infinite number of solutions. However, the reconstruction of the image is still possible, provided that the image has a sparse representation in a certain compression (sparsity) basis Ψ :

$$X = \Psi \cdot F, \quad (3)$$

where F is a vector of coefficients of X in the basis Ψ . The vector F can be either literally sparse, containing only a small number S of non-zero elements, or all the elements apart from the S largest ones can be negligible but still non-zero. In both cases the reconstruction of the image is performed by solving the basis pursuit optimisation problem [1]:

$$\tilde{F} = \arg \min_{F'} \|F'\|_1 \quad \text{subject to} \quad Y = \Phi \cdot \Psi \cdot F' \quad (4)$$

or, in case of noisy data acquisition, the basis pursuit denoise (BPDN) optimisation problem:

$$\tilde{F} = \arg \min_{F'} \|F'\|_1 \quad \text{subject to} \quad \|Y - \Phi \cdot \Psi \cdot F'\|_2 < \varepsilon, \quad (5)$$

where $\|\cdot\|_p$ stands for the ℓ^p norm of a vector and ε represents the level of noise present in the signal. Alternative reconstruction approaches have been also successfully exploited, including minimisation of a certain ℓ^p quasi-norm for $0 \leq p < 1$ [29, 30] or minimisation of the total variation (TV) [31–33].

The sufficient number of measurements required to collect enough data to reconstruct the original image without distortion satisfies the following inequality [34]:

$$m > C \cdot S \cdot \log(n) \cdot \mu^2(\Phi, \Psi), \quad (6)$$

in which C is a small constant, S is the number of relevant coefficients in the compressed image F , and $\mu(\Phi, \Psi)$ is the mutual coherence of the sensing matrix Φ and the sparsity basis Ψ defined as:

$$\mu(\Phi, \Psi) = \sqrt{n} \cdot \max_{j,k} |\langle \phi_j, \psi_k \rangle|, \quad (7)$$

where ϕ_j, ψ_k (for $1 \leq j \leq m$ and $1 \leq k \leq n$) stand for the row vectors of the matrices Φ and Ψ respectively. Therefore, to recover the original image from the least possible number of measurements, it is crucial to choose the sensing matrix Φ in such a manner, that the mutual coherence $\mu(\Phi, \Psi)$ is kept as small as possible. In other words, the sensing matrix should be almost completely incompressible in the basis Ψ .

3 Noiselet matrices

In 2001 a family of functions was introduced, named noiselet functions [28], which is perfectly incoherent with the Haar wavelet basis (mutual coherence between noiselet and Haar orthonormal basis equals 1). Since most of the real-life images are well compressible in the Haar wavelet domain, noiselets are then a good candidate for constructing an efficient sensing matrix.

Another advantage of the discrete noiselet-based sensing matrices over e.g. the Gaussian random matrices is that they are defined using a recursive formula based on the Kronecker product \otimes (a similar formula was introduced in [35]):

$$N_1 = [1], \quad N_{2n} = \frac{1}{2} \begin{bmatrix} 1-i & 1+i \\ 1+i & 1-i \end{bmatrix} \otimes N_n, \quad (8)$$

where N_n are $n \times n$ unitary matrices whose dimension is a power of two $n = 2^q$ (for $q = 0, 1, 2, \dots$). It is worth mentioning, that Eq. (8) defines the matrices of both one-dimensional and two-dimensional noiselet transforms. Indeed, the 2D noiselet transform of a $n \times k$ matrix A takes the form:

$$[N_{n \times k}^{2D}] \cdot \text{vec}(A) = \text{vec}(N_n \cdot A \cdot N_k^T) = (N_k \otimes N_n) \cdot \text{vec}(A) = [N_{n \times k}] \cdot \text{vec}(A), \quad (9)$$

where $\text{vec}(A)$ denotes vectorisation of matrix A obtained by stacking all columns of A into a single column vector. The second equality in Eq. (9) is a well known property of the Kronecker product: $\text{vec}(ABC^T) = (C \otimes A)\text{vec}(B)$ for matrices A, B, C , whereas the last equality is a straightforward consequence of the associativity of the Kronecker product,

which is recursively used to construct the noiselet matrices (see Eq. (8)).

Therefore, the operation of multiplication by a noiselet matrix is replaceable with a fast transform with a computational complexity of $\mathcal{O}(n \log n)$ for both one-dimensional and two-dimensional transforms. Additionally, the huge $n \times n$ noiselet matrix is actually never constructed during the evaluation of the matrix-vector product and hence does not need to be stored in computer memory.

Ignoring the normalizing factors, the elements of the noiselet matrices take discrete values from one of two 4-element sets, depending on the parity of the parameter q defining the size of the matrix $N_n = N_{(2^q)}$:

$$\begin{aligned} \sqrt{n} \cdot N_n(j, k) &\in \{1, -1, i, -i\} && \text{for even } q \\ \sqrt{2n} \cdot N_n(j, k) &\in \{1+i, 1-i, -1+i, -1-i\} && \text{for odd } q, \end{aligned} \quad (10)$$

where $1 \leq j, k \leq n$ are indices of an element of the matrix N_n .

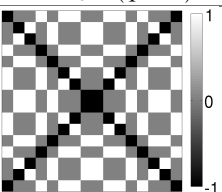
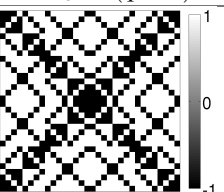
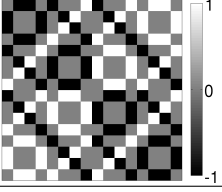
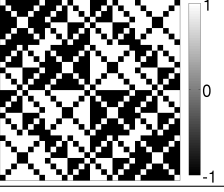
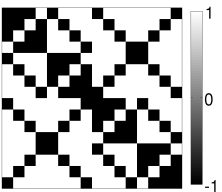
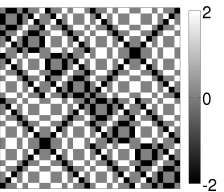
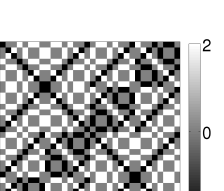
Owing to these properties, noiselet matrices have an excellent potential of being used as the sensing matrices in CS imaging systems. However, displaying complex-valued patterns with the use of the DMD is impossible, or at least not straightforward. A solution to this problem was proposed recently [36], suggesting to divide the complex-valued sensing matrix into four separate matrices, namely: 1. the positive real part, 2. the negative real part, 3. the positive imaginary part, and 4. the negative imaginary part, and to perform the measurements with each of these matrices independently. Then, the collected data may be synthesized into an equivalent of a single sequence of measurements obtained with the complex-valued sensing matrix. This method however, suffers from that the number of snapshots taken by the SPC is fourfold larger than the number of samples actually measured, unnecessarily prolonging the data acquisition time. Instead, we want to replace the complex noiselet functions with the same number of real binary functions, but to retain the incoherence of the basis with Haar wavelets.

In conclusion we note that the definition of discrete noiselet transform is very similar to that of Walsh-Hadamard transform, which also shares the same form for one-dimensional and two-dimensional case, has a similar fast calculation method, and is also commonly used in CS applications especially that it is readily binary. However, the mutual coherence of Walsh-Hadamard matrices with Haar wavelets is much larger.

4 Efficient method of displaying noiselet-based sensing matrices

We propose an efficient method of displaying noiselet-based sensing matrices with the use of a DMD for the purpose of compressive imaging. The method allows for obtaining m complex-valued measurement samples by modulating the object with exactly $m + 1$ real binary patterns. We note, that in general the DMDs enable displaying also grayscale patterns with multiple intensity levels by flickering of the micromirrors, however the use of binary patterns is the most efficient in terms of the frequency of pattern exposure and the stability of the displayed images.

Table 1: Examples of noiselet matrices N_{2^q} with either even or odd value of parameter q .

	$4 \cdot N_{16} \quad (q = 4)$	$8 \cdot N_{32} \quad (q = 5)$
Real part		
Imaginary part		
Sum of real and imaginary parts		
Difference of real and imaginary parts		

The proposed procedure takes the following general form:

1. The sensing matrix Φ is composed of m rows chosen randomly from a complex-valued noiselet matrix N_n .
2. A real binary matrix P (further in this paper called a pattern matrix) is defined, whose rows are linear functions of the rows of matrix Φ .
3. A series of measurements \tilde{Y} is taken by the SPC using the row vectors p_j of the matrix P as the patterns displayed by the DMD:

$$\tilde{Y} = P \cdot X. \quad (11)$$

4. The complex-valued vector Y is calculated from the measurements \tilde{Y} and used for reconstructing the image X .

In order to establish the form of the matrix P we exploit several properties of the noiselet matrices. First we note, that for odd values of parameter q , real and binary patterns are obtained immediately from the real and imaginary part of the noiselet matrix N_{2^q} (see Eq. (10)). For even values of the parameter q , the real and the imaginary part of a noiselet matrix are triple-valued, however binary patterns are obtained from their sum and difference instead. For better illustration, two examples of a noiselet matrix with either even or odd value of the parameter q are presented in Table 1.

However, thus obtained set of patterns suffers from two important shortcomings: 1. the number of real-valued patterns to be displayed by the DMD is twice as large as the number of complex-valued patterns, which they represent and 2. the patterns consist of both positive and negative values. We shall address these issues consecutively.

We begin with the first. This problem may be solved by exploiting the symmetry of the noiselet matrices. Noiselet matrices, similarly to discrete Fourier transform matrices, obey the reflection symmetry of the form:

$$\forall_{1 \leq j, k \leq n} N_n^*(j, k) = N_n(n+1-j, k), \quad (12)$$

where the symbol $*$ denotes the complex conjugate. In other words, each element taken from the upper half of a noiselet matrix N_n (see Fig. 2(a)) is a complex conjugate of the respective mirror element taken from the lower half of the matrix.

Indeed, suppose that Eq. (12) is fulfilled for a noiselet matrix N_n . Then, by induction, for the matrix N_{2n} (see Fig. 2(b)), the elements taken from the left half of the matrix satisfy :

$$\begin{aligned} N_{2n}^*(j, k) &= [(1-i)N_n(j, k)]^* = (1+i)N_n^*(j, k) = \\ &= (1+i)N_n(n+1-j, k) = N_{2n}(2n+1-j, k), \end{aligned} \quad (13)$$

where the first and the last equality result from the recursive definition of the matrix N_{2n} (Eq. (8)) and the third equality results from Eq. (12).

Similarly, for the elements from the right half of the matrix N_{2n} :

$$\begin{aligned} N_{2n}^*(j, n+k) &= [(1+i)N_n(j, k)]^* = (1-i)N_n^*(j, k) = \\ &= (1-i)N_n(n+1-j, k) = N_{2n}(2n+1-j, n+k). \end{aligned} \quad (14)$$

Owing to this property, a pair of patterns consisting of the real and of the imaginary part of a single noiselet (i.e. of a single row vector taken from a noiselet matrix) contains full information about two mirror noiselets taken from the upper and the lower half of the noiselet matrix respectively. Therefore, we propose to choose the sensing matrix Φ in such a manner that it consists of $m/2$ rows randomly picked from the upper half of a noiselet matrix N_n and the $m/2$ mirror rows taken from the lower half of the matrix. Then, the number of unique patterns composed of the real and the imaginary parts (or of their sum and difference) of the rows of matrix Φ equals m .

The second problem, concerning patterns consisting of both positive and negative values, is resolved by applying additional rescaling to the patterns. The patterns are already binary, therefore the necessity of displaying negative-valued pixels may be omitted by replacing them with zeros instead. Thus obtained patterns consist of values 0 and 1 only and they are straightforward to be displayed by a DMD. The cost of this rescaling is the necessity of capturing a single additional measurement, independently of the number of patterns m or of the size of image n . To justify this statement let us first analyse the procedure of restoring the complex-valued measurement vector Y from the real-valued measurements \tilde{Y} .

Let us order the row-vectors ϕ_j of the sensing matrix Φ to obey the following formula:

$$\phi_j = \phi_{m+1-j}^*, \quad \text{where } j = 1, 2, 3, \dots, m/2. \quad (15)$$

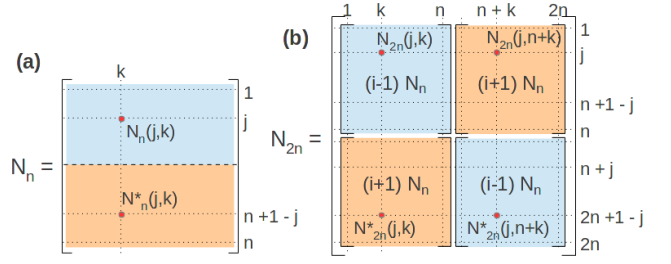


Figure 2: Reflection symmetry of the noiselet matrix. Any element taken from the upper half of the matrix is a complex conjugate of the mirror element taken from the lower half of the matrix. Matrix (b) is obtained from matrix (a) using formula introduced in Eq. 8.

The patterns, i.e. the rows of the proposed pattern matrix P , take one of two forms, depending on the parity of the parameter q defining the size of the sampled image ($n = 2^q$):

for odd q :

$$\begin{aligned} p_{2j-1} &= \frac{1}{2}(\sqrt{2n} \Re(\phi_j) + 1), \\ p_{2j} &= \frac{1}{2}(\sqrt{2n} \Im(\phi_j) + 1), \end{aligned}$$

for even q :

$$\begin{aligned} p_{2j-1} &= \frac{1}{2}(\sqrt{n} [\Re(\phi_j) + \Im(\phi_j)] + 1), \\ p_{2j} &= \frac{1}{2}(\sqrt{n} [\Re(\phi_j) - \Im(\phi_j)] + 1), \end{aligned} \quad (16)$$

where $j = 1, 2, 3, \dots, m/2$.

In both cases, all the patterns stored in the matrix P are real and consist of zeros and ones only.

Simultaneously, the row vectors of the sensing matrix Φ are expressed in terms of the patterns p_{2j-1}, p_{2j} by the following equations:

for odd q :

$$\phi_j = \frac{1}{\sqrt{2n}} (2p_{2j-1} + 2ip_{2j} - (1+i)),$$

for even q :

$$\phi_j = \frac{1}{\sqrt{n}} ((1+i)p_{2j-1} + (1-i)p_{2j} - 1),$$

where $j = 1, 2, 3, \dots, m/2$.

Finally, the equivalents of the complex-valued measurements y_j are restored from the actual real-valued measurements \tilde{y}_k using the following formulas:

for odd q :

$$\begin{aligned} y_j &= y_{m+1-j}^* = \langle \phi_j, X \rangle = \\ &= \frac{1}{\sqrt{2n}} \left(2\langle p_{2j-1}, X \rangle + 2i\langle p_{2j}, X \rangle - (1+i)\langle I_v, X \rangle \right) = \\ &= \frac{1}{\sqrt{2n}} \left(2\tilde{y}_{2j-1} + 2i\tilde{y}_{2j} - (1+i)\langle I_v, X \rangle \right), \end{aligned}$$

for even q :

$$\begin{aligned} y_j &= y_{m+1-j}^* = \langle \phi_j, X \rangle = \\ &= \frac{1}{\sqrt{n}} \left((1+i) \langle p_{2j-1}, X \rangle + (1-i) \langle p_{2j}, X \rangle - \langle I_v, X \rangle \right) = \\ &= \frac{1}{\sqrt{n}} \left((1+i) \tilde{y}_{2j-1} + (1-i) \tilde{y}_{2j} - \langle I_v, X \rangle \right), \end{aligned} \quad (18)$$

where $j = 1, 2, 3, \dots, m/2$,

and I_v denotes a vector of length n with all elements equal to 1. The term $\langle I_v, X \rangle$, which occurs in both cases in Eq. (18), is the consequence of the rescaling applied to the patterns in order to obtain only non-negative values. In physical interpretation, this term represents a measurement of the total intensity of the image X without modulating it with any pattern. This single additional measurement is necessary for reverting the scaling during retrieval of Y . Therefore, exactly $m+1$ measurements with real binary and non-negative patterns are required in order to restore m samples corresponding to measurements taken with a complex-valued and non-binary noiselet-based sensing matrix.

In practical experimental conditions this number of measurements may be increased. For instance, in order to eliminate the background ‘dark pixel’ signal resulting from the light reflected from the DMD matrix when all the mirrors are in the off-state, it is necessary to measure that dark signal in the calibration stage, and then to subtract it from the measurements. More likely, the intensity of the light-source may vary with time. An additional detector could be used for the normalization of measurements [5]. In another approach, a differential measurement with complementary [37] binary masks $(\langle p_k, X \rangle - \langle I_v - p_k, X \rangle)/2$ increases the signal-to-noise-ratio, eliminates background dark signal, and accounts for intensity variations but actually doubles the number of measurements.

5 Modification of the fast noiselet transform for real-time generation of the noiselet-based patterns

In the following section we propose a modification of the fast noiselet transform for the purpose of efficient generation of the noiselet-based real binary patterns introduced in Section 4. The one-dimensional and two-dimensional noiselet transform defined by Eq. (8) operates on complex numbers. We propose a similar procedure, allowing for a direct generation of the real binary patterns p_j using only operations of summation and subtraction on integer variables. Moreover, by utilising the bit representation of a k -bit integer, a bundle of up to $k-2$ patterns p_j may be generated using the same number of arithmetic operations as in the case of generating only a single pattern (the additional two bits are used in the intermediate calculations). The efficiency of the proposed method allows for generating the patterns p_j during the time of the experiment, without any preparations beforehand.

The modified noiselet transform matrix \tilde{N}_n (where $n = 2^q$) relates to the noiselet matrix N_n as follows:

$$\tilde{N}_n = \sqrt{2n} \cdot N_n \exp(i\frac{\pi}{4}(q+1)) \quad (19)$$

and it satisfies a recursive formula similar to that, which defines matrices N_n :

$$\begin{aligned} \tilde{N}_1 &= [1+i], \\ \tilde{N}_{2n} &= \begin{bmatrix} 1 & i \\ i & 1 \end{bmatrix} \otimes \tilde{N}_n. \end{aligned} \quad (20)$$

We note, that the elements of thus defined matrix \tilde{N}_n belong to a single 4-element set, independently on the parameter q :

$$\tilde{N}_n(j, k) \in \{1+i, 1-i, -1+i, -1-i\}. \quad (21)$$

To derive the modified noiselet transform $\tilde{\mathcal{N}}$, let us rewrite Eq (20) into a more explicit form. We define an auxiliary matrix:

$$\tilde{N}_G = \begin{bmatrix} 1 & i \\ i & 1 \end{bmatrix}. \quad (22)$$

Then, the modified noiselet matrix takes a form:

$$\begin{aligned} \tilde{N}_{2^q} &= (1+i) \underbrace{\tilde{N}_G \otimes \tilde{N}_G \otimes \dots \otimes \tilde{N}_G}_q = \\ &= (1+i) (\tilde{N}_G \otimes I_2 \otimes \dots \otimes I_2) \cdot \\ &\quad \cdot (I_2 \otimes \tilde{N}_G \otimes I_2 \otimes \dots \otimes I_2) \dots (I_2 \otimes \dots \otimes I_2 \otimes \tilde{N}_G) = \\ &= (1+i) (\tilde{N}_G \otimes I_{2^{q-1}}) (I_2 \otimes \tilde{N}_G \otimes I_{2^{q-2}}) \dots (I_{2^{q-1}} \otimes \tilde{N}_G), \end{aligned} \quad (23)$$

where I_n stands for an identity matrix of size $n \times n$, and the second equality results from the mixed-product property of the Kronecker product: $(A \otimes B)(C \otimes D) = (AC) \otimes (BD)$. Each factor in the final expression in Eq. (23) of a form $I_{2^{k-1}} \otimes \tilde{N}_G \otimes I_{2^{q-k}}$ for $k = 1, 2, \dots, q$, is a block diagonal matrix with 2^{k-1} same blocks of the form:

$$\tilde{N}_G \otimes I_{2^{q-k}} = \begin{bmatrix} I_{2^{q-k}} & i I_{2^{q-k}} \\ i I_{2^{q-k}} & I_{2^{q-k}} \end{bmatrix}. \quad (24)$$

Therefore, the modified noiselet transform of a vector (i.e. the multiplication of the vector by the matrix \tilde{N}_{2^q}) is equivalent to dividing the vector into 2^{k-1} blocks, each of length 2^{q-k+1} , and multiplying each of them by the matrix (24). The procedure is then repeated q times for sizes of the blocks defined by consecutive values of k . The product of a single partial vector $v = \begin{bmatrix} u \\ w \end{bmatrix}$ by the matrix (24) has a simple form:

$$\begin{bmatrix} I_{2^{q-k}} & i I_{2^{q-k}} \\ i I_{2^{q-k}} & I_{2^{q-k}} \end{bmatrix} \begin{bmatrix} u \\ w \end{bmatrix} = \begin{bmatrix} u+iw \\ w+iu \end{bmatrix}, \quad (25)$$

which, by keeping the real and the imaginary parts of the vectors as separate variables, does not require any implementation of complex numbers. Moreover, the only arithmetical operations present in the transform are summations and subtractions applied to the real and the imaginary part of the vector v . Therefore, for vector v consisting only of integer values, the transform may be implemented purely on integer types, which greatly increases its efficiency.

The real binary patterns P introduced in the previous section are obtained directly from the modified noiselet transform. Indeed, if a complex sensing pattern ϕ_j is chosen as the k -th row of the noiselet matrix N_n , then the pair of its equivalent real binary patterns p_{2j-1} , p_{2j} defined by Eq. (19) is

expressed by the modified noiselets as follows:

$$\begin{aligned} &\text{for } q \bmod 4 \geq 2 \\ &\quad p_{2j-1} = \pm a_k, \\ &\quad p_{2j} = \pm b_k, \\ &\text{for } q \bmod 4 < 2 \\ &\quad p_{2j-1} = \pm b_k, \\ &\quad p_{2j} = \pm a_k, \quad j = 1, 2, 3, \dots, m/2, \end{aligned} \quad (26)$$

where

$$\begin{aligned} a_k &= \frac{1}{2}(\Re(\tilde{\mathcal{N}}_{n,k}) + 1), \\ b_k &= \frac{1}{2}(\Im(\tilde{\mathcal{N}}_{n,k}) + 1), \end{aligned} \quad (27)$$

$\tilde{\mathcal{N}}_{n,k}$ indicates the k -th row of the matrix $\tilde{\mathcal{N}}_n$ and $q \bmod a$ stands for the remainder after division of parameter q by a . The signs in the expressions for p_{2j-1} , p_{2j} depend on the value of the complex argument in Eq. (19).

Now, let us explain the operation of the packed modified noiselet transform. A single pattern a_k or b_k is efficiently obtained by applying the modified noiselet transform to a unit vector e_k , whose all elements apart from the k -th one are zeros:

$$\begin{aligned} a_k &= \frac{1}{2}\Re(\tilde{\mathcal{N}}(e_k) + 1), \\ b_k &= \frac{1}{2}\Im(\tilde{\mathcal{N}}(e_k) + 1). \end{aligned} \quad (28)$$

The operation required to obtain a bundle of different binary patterns a_{k_j} (or b_{k_j} with interchanging $\Re \leftrightarrow \Im$) encoded into the consecutive bit-planes of the bit representation of the integer variables is derived from Eq. (28):

$$\begin{aligned} a_{\text{packed}} &\equiv \sum_{j=1}^l 2^j a_{k_j} = \sum_{j=1}^l 2^j \frac{1}{2}\Re(\tilde{\mathcal{N}}(e_{k_j}) + 1) = \\ &= \frac{1}{2}\Re\left[\tilde{\mathcal{N}}\left(\sum_{j=1}^l 2^j e_{k_j}\right) + \sum_{j=1}^l 2^j\right] = \\ &= \frac{1}{2}\Re(\tilde{\mathcal{N}}(e_{\text{packed}}) + 2^{l+1} - 1), \end{aligned} \quad (29)$$

where $e_{\text{packed}} = \sum_{j=1}^l 2^j e_{k_j}$ is a vector composed of a bundle of unit vectors e_{k_j} encoded into the consecutive bit-planes of its integer elements. From Eqs. (28), (29) one may easily determine that the computational complexity of calculating the whole bundle of patterns is identical as in the case of calculating a single pattern. The number of patterns, which may be calculated with a single run of the modified noiselet transform, is limited only by the bit-width of the integer variables used in the implementation of the transform.

To illustrate the efficiency of the modified noiselet transform, we note that our C++ implementation of the transform generates around 110 bundles of patterns of resolution 512×512 per second or 250 bundles of patterns of resolution 256×256 per second on a mid-range laptop. For patterns bundled into packages of 24, as is the case in our experiment, this is respectively 2700 or 6000 patterns per second. This speed already includes all the operations on the computer graphical objects and hardware necessary to display the patterns.

6 Experimental Results

We will now demonstrate the experimental results of reconstructing an image captured by a SPC. We apply binary sam-

pling equivalent to noiselet sampling according to the procedure proposed in Sections 4 and 5.

6.1 Design of the experimental setup

The schematic of our experimental system matches the one shown in Fig. 1. We use a DMD light modulator (TI DLP LightCrafter 4500) integrated with an RGB LED light source and optical lens to project the sampling patterns onto the object plane. The DMD consists of 912×1140 square micromirrors organised into a diamond grid, i.e. a square grid rotated by 45° with respect to the boundaries of the DMD. Out of this array, we use a square sub-area of 512×512 pixels oriented along the edges of the pixels, so that the boundaries of the area form straight lines. All the patterns are transformed in order to be displayed in this area, which ensures accurate projection of the patterns into a square grid, without distortions resulting from the diamond pixel layout of the device. A similar approach was previously reported in [38]. The single-pixel detector consists of a photodiode integrated with an on-chip transimpedance amplifier (TI OPT-101P) with peak sensitivity wavelength of 650 nm. The analog signal is digitized with a 16-bit A/D converter (NI USB-6003 100kS/s multifunction DAQ) and streamed to a PC via USB port. Data acquisition is controlled with a LabView routine.

The DLP displays binary patterns consisting of arbitrarily selected bit-planes of 24-bit RGB images. These images may be either first stored in the internal flash memory or streamed via HDMI video port. The latter solution is more convenient, since it does not impose memory restrictions and allows for a more flexible choice of patterns, by generating them in real time during the measurements instead of preparing and uploading them beforehand. We have developed a dedicated fast routine in C++ based on modified noiselet transform (see Section 5) to generate noiselet-based patterns (Eq. (26)) bundled together in packages of 23 (with one bit left for synchronization) into the bit-representations of RGB images. Such images are transferred through HDMI port to the DLP and then displayed in sequence, bit by bit. Our system is capable of displaying binary patterns at the maximum rate of 1440 Hz ($24 \text{ bits} \times 60 \text{ Hz}$ of the video rate). However, the actual speed of displaying the patterns in the experiment is set to 240 Hz in order to preserve high signal to noise ratio and to ensure stability of the data acquisition.

The accuracy of the measurements is an important issue for the SPC imaging. Since all the noiselet-based binary patterns of the same resolution have the same total brightness, the standard deviation of the measurements taken with different patterns is usually at least two orders of magnitude smaller than their average value. Therefore, in order to increase the signal to noise ratio and to reduce the influence of both the background signal from the dark pixels and the light intensity variations over time, we use the technique of differential measurements, involving displaying both the patterns and their binary negations. In a different SPC design, similar effect could be obtained without doubling the number of measurements, by introducing a second detector to measure synchronously the total intensity of light reflected from the DMD.

Finally, we recover the image from the measured data by solving the BPDN problem (see Eq. (5)) with the use of the

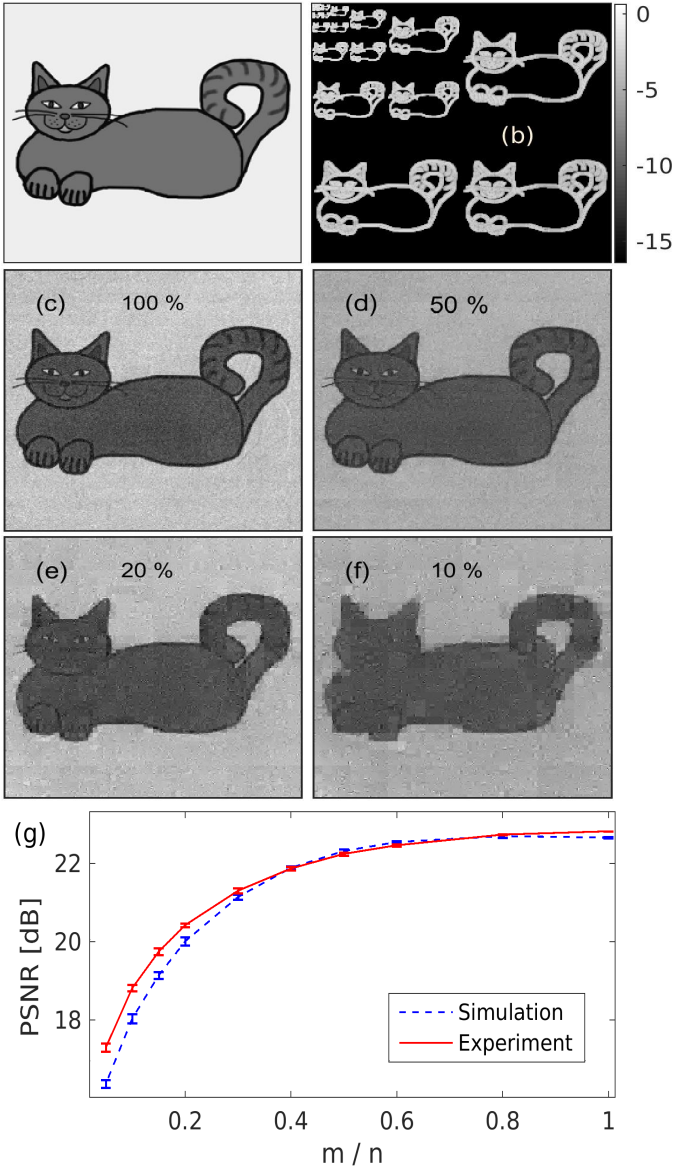


Figure 3: Experimental demonstration of compressive imaging with SPC using noiselet-based sensing patterns with resolution 256×256 : (a) the original image, (b) two-dimensional Haar wavelet transform of (a) (logarithmic scale), (c-f) recovery of the image from the experimental data using different sampling ratios m/n between 100% (a) and 10% (d), (g) experimental and theoretical PSNR as a function of the sampling ratio m/n . The errorbars in (g) refer to the standard deviation calculated over 40 (for $m/n \leq 0.3$) or 20 (for $0.3 < m/n < 1$) randomly chosen sets of the sampling patterns with the same value of the sampling ratio m/n .

SPGL1 package [39]. In the worst case scenario of recovering an image from measurements with 50% elements of the noiselet basis, the optimisation takes approximately 3 s for an image with resolution 256×256 (in Matlab, using a PC with a single eight-core processor). In the case of reconstructing the image from the entire noiselet basis, a straightforward approach of calculating the inverse noiselet transform may be applied, reducing the time of recovery to 0.03 s.

6.2 Results

The original image used for the experiment is presented in the Fig. 3(a). The image is well compressible in the Haar wavelets, as shown in Fig. 3(b), with only 24% of non-zero Haar coefficients. Further lossy compression is also possible, with the peak signal to noise ratio (PSNR, see Eq. (30)) of the compressed image on the order of 40 dB when 8% of the largest Haar coefficients are preserved.

The image is sampled with the noiselet-based real binary patterns of the resolution $n = 256 \times 256$. The recovery of the image is repeated using several different values of the sampling ratio m/n from the range between 5% and 100%, where 100% corresponds to the sensing matrix Φ consisting of all possible noiselets from a single noiselet matrix. Several examples of reconstructed images obtained with different values of the sampling ratio are presented in Figs. 3(c)-(f). Additionally, in Fig. 3(g) we present how the sampling ratio influences the accuracy of reconstruction of the image. To measure the quality of the reconstruction, we use the PSNR defined as:

$$\text{PSNR} = 10 \log_{10} \left(\frac{[\max(X)]^2}{\text{MSE}(\tilde{X})} \right), \quad (30)$$

where \tilde{X} represents distribution of brightness in the reconstructed image, $\max(X)$ stands for the peak brightness of the original image, and $\text{MSE}(\tilde{X}) = \frac{1}{n} \sum_{i=1}^n (\tilde{X}_i - X_i)^2$ is the mean squared error of the reconstructed image as compared to the original one. Before calculating the PSNR, both images have been registered and normalised in order to match their intensity levels. We note that PSNR is not a deterministic function of the sampling ratio - it depends on the specific patterns used in the measurement or simulation. Therefore, in Fig. 3(g) we show also the standard deviation of PSNR calculated over a number of randomly chosen sets of patterns with the same value of the sampling ratio.

We define the experimental noise as the difference between the measured and calculated values of \tilde{Y} . The standard deviation of the experimental noise is on the order of 0.0004 of the mean value of the measured signal and it is by approximately two orders of magnitude lower than the peak-to-peak amplitude of the measurements taken with different patterns. By introducing additive Gaussian white noise to the theoretical model of the measurement, we obtain a good agreement between the simulated compressive measurement and the actual experimental results (see Fig. 3(g)).

7 Conclusions

We have proposed theoretically and validated experimentally an efficient method of using complex-valued and non-binary noiselet functions for object sampling in single-pixel cameras with binary spatial light modulators and incoherent illumination. Minimal mutual coherence of discrete noiselets and Haar wavelets makes this pair of bases an essential choice for the sensing and compression matrices in compressed sensing with single-pixel detectors. Indeed, most real-world images are compressible in the Haar basis. The proposed method allows to determine m noiselet coefficients from $m + 1$ binary

sampling measurements. Moreover, we have proposed a modification to the complex fast noiselet transform, which enables computationally-efficient generation of the binary noiselet-based patterns using only operations of summation and subtraction on integer variables. Further acceleration is obtained by utilising the bit representation of a k -bit integer to calculate a bundle of up to $k-2$ patterns without any additional computational cost as compared with generating only a single pattern. The efficiency of the proposed method allows for generating patterns in real time on a PC or even on a single-board computer.

Funding Information

Funding. We acknowledge financial support from the National Science Centre, Poland grant UMO-2014/15/B/ST7/03107 and European Union Seventh Framework Programme (FP7/2007-2013, grant agreement no 316244).

References

- [1] E. J. Candes and M. B. Wakin. An Introduction To Compressive Sampling. *IEEE Signal Processing Mag.*, 25:21–30, 2008.
- [2] M. Foucart and H. Rauhut. *A mathematical introduction to compressive sensing*. Springer, 2013.
- [3] J. H. Shapiro. Computational ghost imaging. *Phys. Rev. A*, 78(061802), 2008.
- [4] Y. Bromberg, O. Katz, and Y. Silberberg. Ghost imaging with a single detector. *Phys. Rev. A*, 79:053840, 2009.
- [5] B. Sun, S. S. Welsh, M. P. Edgar, J. H. Shapiro, and M. J. Padgett. Normalized ghost imaging. *Opt. Express*, 20(15):16892–16901, 2012.
- [6] M. F. Duarte, M. A. Davenport, D. Takhar, J. N. Laska, T. Sun, K. F. Kelly, and R. G. Baraniuk. Single-Pixel Imaging via Compressive Sampling. *IEEE Signal Processing Mag.*, 25:83–91, 2008.
- [7] M. E. Gehm and D. J. Brady. Compressive sensing in the EO/IR. *Appl. Opt.*, 54:C14, 2015.
- [8] L. Chan, K. Charan, D. Takhar, K. F. Kelly, R. G. Baraniuk, and D. M. Mittelman. A single-pixel terahertz imaging system based on compressed sensing. *Appl. Phys. Lett.*, 93:121105, 2008.
- [9] C. M. Watts, D. Shrekenhamer, J. Montoya, G. Lipworth, J. Hunt, T. Sleasman, S. Krishna, D. R. Smith, and W. J. Padilla. Terahertz compressive imaging with metamaterial spatial light modulators. *Nature Photon.*, 8:605–609, 2014.
- [10] L. Qiao, Y. Wang, Z. Shen, Z. Zhao, and Z. Chen. Compressive sensing for direct millimeter-wave holographic imaging. *Appl. Opt.*, 54:3280, 2015.
- [11] S. S. Welsh, M. P. Edgar, R. Bowman, P. Jonathan, B. Sun, and M. J. Padgett. Fast full-color computational imaging with single-pixel detectors. *Opt. Express*, 21(20):23068, 2013.
- [12] M. E. Gehm, R. John, D. J. Brady, R. M. Willett, and T. J. Schulz. Single-shot compressive spectral imaging with a dual-disperser architecture. *Opt. Express*, 15:14013, 2007.
- [13] V. Duran, P. Clemente, M. Fernandez-Alonso, E. Tajahuerce, and J. Lancis. Single-pixel polarimetric imaging. *Opt. Lett.*, 37:824, 2012.
- [14] J. Busck and H. Heiselberg. Gated viewing and high-accuracy three-dimensional laser radar. *Appl. Opt.*, 43:4705, 2004.
- [15] L. Li, W. Xiao, and W. Jian. Three-dimensional imaging reconstruction algorithm of gated-viewing laser imaging with compressive sensing. *Appl. Opt.*, 53:7992, 2014.
- [16] M. Chao, A. Mahalanobis, and B. Javidi. 3d passive integral imaging using compressive sensing. *Opt. Express*, 20:26624, 2012.
- [17] B. Sun, M. P. Edgar, R. Bowman, L. E. Vittert, S. S. Welsh, A. Bowman, and M. J. Padgett. 3D Computational Imaging with Single-Pixel Detectors. *Science*, 340:844–847, 2013.
- [18] C. Zhao, W. Gong, M. Chen, E. Li, H. Wang, W. Xu, and S. Han. Ghost imaging lidar via sparsity constraints. *Appl. Phys. Lett.*, 101(14):141123, 2012.
- [19] P. Clemente, V. Duran, E. Tajahuerce, P. Andres, V. Clement, and J. Lancis. Compressive holography with a single-pixel detector. *Opt. Lett.*, 38:2524, 2013.
- [20] Y. Rivenson, A. Stern, and B. Javidi. Overview of compressive sensing techniques applied in holography. *Appl. Opt.*, 52:A423, 2013.
- [21] S. Gazit, A. Szameit, Y. C. Eldar, and M. Segev. Super-resolution and reconstruction of sparse sub-wavelength images. *Opt. Express*, 17(26):23920, 2009.
- [22] Y. Shechtman, Y. C. Eldar, A. Szameit, and M. Segev. Sparsity based sub-wavelength imaging with partially incoherent light via quadratic compressed sensing. *Opt. Express*, 19(16):14807, 2011.
- [23] D. Pastor-Calle, A. Pastuszczak, M. Mikolajczyk, and R. Kotynski. Compressive phase-only filtering at extreme compression rates. arXiv:1604.07751.
- [24] M. Lusting, D. L. Donoho, J. M. Santos, and J. M. Pauly. Compressed Sensing MRI. *IEEE Signal Processing Mag.*, 25:72–82, 2008.
- [25] L. Weizman, Y. C. Eldar, and D. Ben Bashat. Compressed Sensing for Longitudinal MRI: An Adaptive-Weighted Approach. *Medical Physics*, 42(9):5195–5208, 2015.
- [26] V. Duran, F. Soldevilla, E. Irlas, P. Clemente, E. Tajahuerce, P. Andres, and J. Lancis. Compressive imaging in scattering media. *Opt. Express*, 23(11):14424, 2015.
- [27] M. P. Edgar, G. M. Gibson, R. Bowman, B. Sun, N. Radwell, K. J. Mitchell, S. S. Welsh, and M. J. Padgett. Simultaneous real-time visible and infrared video with single-pixel detectors. *Scientific Reports*, 52:10669, 2015.
- [28] R. Coifman, F. Geshwind, and Y. Meyer. Noiselets. *Applied and Computational Harmonic Analysis*, 10:27–44, 2001.
- [29] R. Chartrand. Exact reconstruction of sparse signals via nonconvex minimization. *IEEE Signal Process. Lett.*, 14(10):707–710, 2007.

- [30] R. Chartrand and V. Staneva. Restricted isometry properties and nonconvex compressive sensing. *Inverse Problems*, 24(3), 2008.
- [31] T. F. Chan, J. Shen, and H. M. Zhou. Total variation wavelet inpainting. *Journal of Mathematical Imaging and Vision*, 25(1):107–125, 2006.
- [32] D. Needell and R. Ward. Stable Image Reconstruction Using Total Variation Minimization. *SIAM J. Imaging Sci.*, 6(2):1035–1058, 2013.
- [33] S. Ma, W. Yin, Y. Zhang, and A. Chakraborty. An Efficient Algorithm for Compressed MR Imaging using Total Variation and Wavelets. In *Computer Vision and Pattern Recognition, IEEE Conference on*, 2008.
- [34] E. Candes and J. Romberg. Sparsity and incoherence in compressive sampling. *Inverse Problems*, 23:969–985, 2007.
- [35] T. Tuma and P. Hurley. On the incoherence of noiselet and Haar bases. <http://dsp.rice.edu/sites/dsp.rice.edu/files/cs/noiselets.pdf>.
- [36] M. Zhao, J. Liu, S. Chen, C. Kang, and W. Xu. Single-pixel imaging with deterministic complex-valued sensing matrices. *J. Eur. Opt. Soc. - Rapid*, 10(15041), 2015.
- [37] W.-K. Yu, X.-R. Yao, X.-F. Liu, L.-Z. Li, and G.-J. Zhai. Three-dimensional single-pixel compressive reflectivity imaging based on complementary modulation. *Appl. Opt.*, 54:363, 2015.
- [38] A. D. Rodriguez, P. Clemente, E. Tajahuerce, and J. Lancis. Dual-mode optical microscope based on single-pixel imaging. *Opt. Lasers Eng.*, 82:8794, 2016.
- [39] E. van den Berg and M. P. Friedlander. Sparse optimization with least-squares constraints. *SIAM J. on Optimization*, 21(4):1201–1229, 2011.